Chapter III

Characterization of Electroabsorption Modulator based on InGaAlAs/InGaAlAs Multi-quantum Wells

3.1 Simulation of the MQW Electroabsorption Modulator

In order to study the feasibility of the fabrication and the primary characteristic of EAM, the simulations of the MQW structure have firstly been studied. Because the core parameters of this research rely on the EA effect, it is necessary to know the device absorption coefficient spectra as the evidence of QCSE. For in our work, we care much about the cross absorption modulation (XAM) and cross phase modulation (XPM), the refractive index change due to the carrier density should also be analyzed.

Our simulation is based on the K.P theory and Luttinger-Kohn's model. The following shows the main results in the calculation [1].

Band-to-band absorption [2] [3]

The absorption coefficient $\alpha_B(\hbar\omega)$ is obtained by summing over each of the individual band-to-band absorption transitions. Thus

$$\alpha_B(\hbar\omega) = \sum_{m,l} \alpha_{m,l}(\hbar\omega) \tag{3.1}$$

where $\alpha_{m,l}(\hbar\omega)$, the band-to-band transition from *m*th valence subband to *l*th conduction subband, is given by

$$\alpha_{m,l}(\hbar\omega)=\frac{\pi e^2\hbar}{\varepsilon_0 n_0 c m_0{}^2 L_w}\left(\frac{1}{\hbar\omega}\right)\sum_{\sigma=U,L}\sum_{\mathbf{k}_t}\left|\mathbf{e}\cdot\mathbf{P}^{\sigma}_{m,l}(\mathbf{k}_t)\right|^2 L\left(E^{\sigma}_{m}(\mathbf{k}_t)-E^{e}_{l}(\mathbf{k}_t)+\hbar\omega\right) \quad (3.2)$$

where ε_0 is the permitivity of free space, n_0 is refractive index, c is velocity of light in vacuum, L_w is the quantum-well width, L(E) is a Lorenzian function of half width Γ given by

$$L(E)=\frac{\Gamma}{\pi}\frac{1}{E^2+\Gamma^2} \quad (3.3)$$

and

$$\sum_{\mathbf{k}_t}=\frac{1}{2\pi}\int_0^{\infty}k_t dk_t \quad (3.4)$$

Exciton Absorption

The total exciton-absorption coefficient $\alpha_{ex}(\hbar\omega)$ ex is obtained by summing over each of the individual exciton absorptions. Thus

$$\alpha_{ex}(\hbar\omega)=\sum_{m,l}\alpha^{ex}_{m,l}(\hbar\omega) \quad (3.5)$$

where $\alpha^{ex}_{ml}(\hbar\omega)$ is given by

$$\alpha^{ex}_{m,l}(\hbar\omega)=\frac{2\pi e^2\hbar}{\varepsilon_0 n_0 c m_0{}^2 L_w}\frac{1}{E^{ex}_{m,l}}\sum_{\sigma=U,L}\left|\sum_{\mathbf{k}_t}G_{m,l}(\mathbf{k}_t)\mathbf{e}\cdot\mathbf{P}^{\sigma}_{m,l}(\mathbf{k}_t)\right|^2 L\left(E^{ex,\sigma}_{m,l}-\hbar\omega\right) \quad (3.6)$$

The absorption coefficient is often also written in terms of oscillator strengths $f_{m,l}$ as

$$\alpha^{ex}_{m,l}(\hbar\omega)=\frac{\pi e^2\hbar}{\varepsilon_0 n_0 c m_0 L_w}\sum_{\sigma=U,L}f^{\sigma}_{m,l}L\left(E^{ex,\sigma}_{m,l}-\hbar\omega\right) \quad (3.7)$$

where the oscillator strength per unit area is defined by

$$\alpha^{ex}_{m,l}(\hbar\omega)=\frac{2}{m_0}\frac{1}{E^{ex}_{m,l}}\left|\sum_{\mathbf{k}_t}G_{m,l}(\mathbf{k}_t)\mathbf{e}\cdot\mathbf{P}^{\sigma}_{m,l}(\mathbf{k}_t)\right|^2 \quad (3.8)$$

Example: InGaAlAs/InGaAlAs 1.49 um wavelength multi quantum well structure

InGaAlAs/InGaAlAs multi quantum well (MQW) structure composes of bulk lattice-matched

InGaAlAs with the band gap corresponding to the wavelength 1.1 um as the separated carrier hetero-structure (SCH) and barrier layers. The band gap of InGaAlAs wells will be grown by trial and error until the photoluminescence peak of MQW appears around at 1.49 um wavelength. The number of wells typically grown in our laboratory is 10 wells. The structure of the layers can be listed as follow.

- p+-InGaAs ohmic contact layer = 200 nm
- p-InP layer = 1000 nm depending on the optical confinement and losses.
- InGaAsP etching-stop layer = 5-10 nm
- u-InP cladding layer = 100-200 nm depending on the optical confinement.
- Upper InGaAlAs Q1.1 SCH layer = 100 nm
- 10 sets of InGaAlAs/InGaAlAs quantum well, well width = 7 nm, barrier width = 5 nm
- Lower InGaAlAs Q1.1 SCH layer = 100 nm
- n-InP buffer layer = 200 nm
- n+-InP substrate

In this simulation, the thickness of undoped layers (firstly exclude the u-InP cladding layer under the etching-stop layer) will be totally 330 nm. Thus, the applied electric field in this simulation will equal $(V+V_{th})/330$ nm, where V is the applied reverse biased voltage and V_{th} is the build-in electric field. According to the I-V curve of the fabricated device, the V_{th} equals to 0.7V. Thickness of the well is 19 monolayers. The value of x and y of each layers are described in Table 2.1. The band discontinuity in this calculation is set to 70% and 30% of ΔE_g for ΔE_c and ΔE_v, respectively. We can see that the conduction band will have the deep well while the valence band will be shallow. The band diagram of this MQW structure is shown in Figure 3.1. The figure shows the envelope wave functions on their corresponding energies. The plot is in the condition of $k_t = 0$, at zero total electric field, in which the solutions from the upper and lower Hamiltonian matrices of the valence band are degenerate.

Table 3.1 Parameters of MQW structure.

Material	*x*	*y*	*Thickness (monolayer)*
$In_{(1-x-y)}Ga_xAl_yAs$ Barrier	0.206	0.2667	17
$In_{(1-x-y)}Ga_xAl_yAs$ Well	0.4583	0.02	19
$In_{(1-x-y)}Ga_xAl_yAs$ Barrier	0.206	0.2667	17

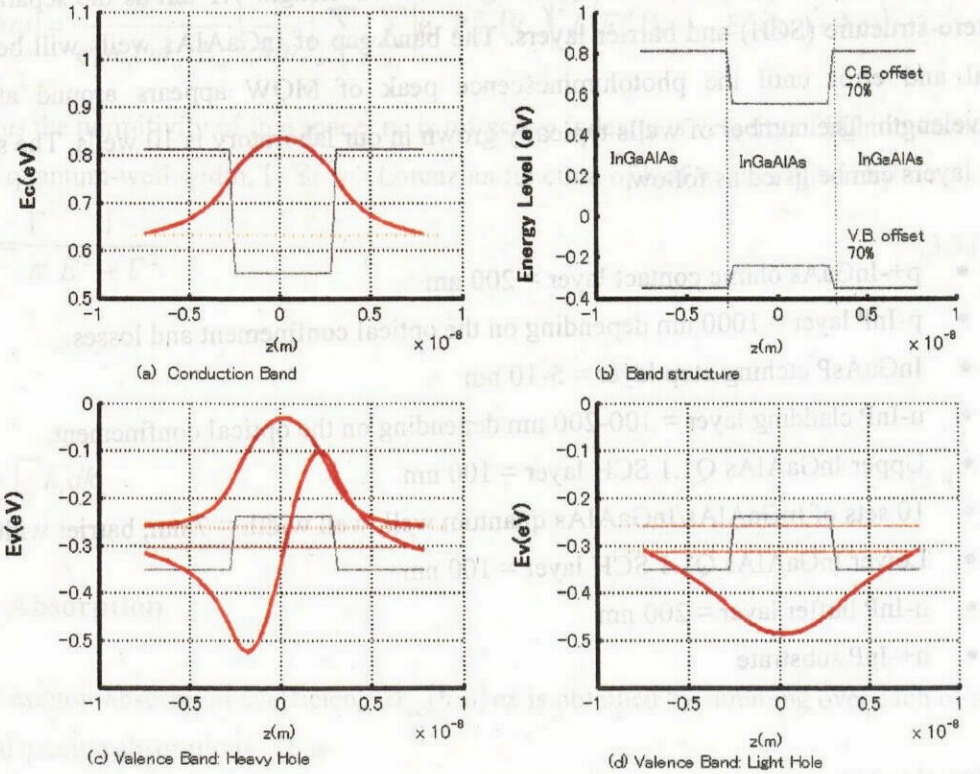

Fig. 3.1 Band structures of InGaAlAs/InGaAlAs MQW structure

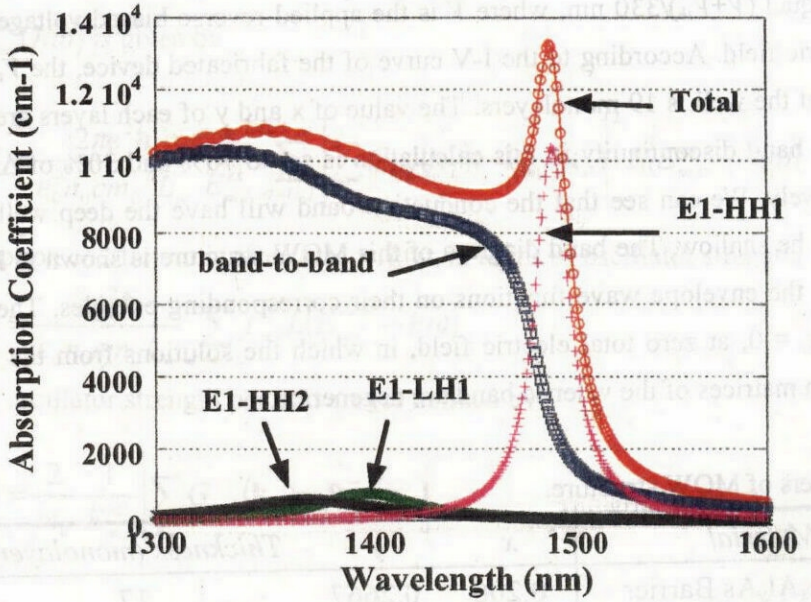

Fig. 3.2 TE Absorption due to exciton resonance of a 7-nm-wide lattice-matched InGaAlAs / InGaAlAs multiple quantum well at 0 V reverse biased voltage (21kV build-in electric field). Band-to-band and total absorptions are also shown.

The simulated envelope functions of electrons and holes will be kept to calculate the absorption coefficient, refractive index change and exciton. Figure 3.2 shows the absorption coefficient spectra of the InGaAlAs/InGaAlAs 1.49 um quantum well for TE mode, including the sole band-to-band transition and several exciton absorption. In our case, the total absorption coefficient is the sum of the band-to-band transition and exciton absorption, without taking the ratio between them into account. The band-to-band absorption involves the one conduction band and two valence bands, as shown in Fig. 3.1(a) (c) (d). In the exciton calculation, we pay attention to only the 1*s* exciton from n^{th} and m^{th} subband of conduction and valence bands, respectively. By making a comparison of band-to-band absorption and exciton peak, it is understood that the exciton peak is observed at the shoulder of band-to-band absorption. A strong E1-HH1 exciton-absorption peak occurs at the absorption edge, and this strong peak plays an important role in MQW EAM.

Figure 3.3 shows the calculated absorption-coefficient spectra of the same MQW for TE polarization, as the function of external applied field. Note that the peaks of E1-HH1 exciton transition shift to long wavelength because of the reduce of the effective band gap energy, and the intensity of the absorption reduce due to the separating of the wave functions of electrons and holes. It denotes the "Quantum Confined Stark Effect" (QCSE) [4]. Because we did not measure the TE-mode photocurrent of the fabricated device with the same parameters used in the simulation, we do not know how much the simulation matches with the experimental results. However, the wavelength shift of E1-HH1 transition in the simulation due to the exciton absorption does match quite well with the experiments shown in Fig.3.9.

Fig. 3.4 shows the calculated absorption coefficient spectra changes with the carrier density in the same quantum well for TE mode. Fig.3.4 (a) shows the results for band-to-band transitions. The coefficient reduces as the carrier density increases according to the band-filling effect. One interesting thing has been found that the quantum well changes from conventionally absorptive media to abnormal media with gain at the wavelengths between 1450nm to 1500nm. Actually this phenomenon is quite ordinary in semiconductor optical amplifier (SOA). In SOA, the carrier density comes from the injection current. If by some means, the carrier density can be controlled not only electrically, but also optically, the absorptive medium can be made to be with gain. This is the origin of our proposal shown in Chapter VII. Fig.3.4 (b) shows the results for only the exciton transitions. We can see that the exciton peak will be lower and shift to the shorter wavelength as the carrier density increases. So, not only the decrement of the peaks own but also the peak shifting will reduce the absorption at the absorption edge as the carrier density

increase. Combining both the band-to-band transitions and exciton transitions, we can get the total absorption coefficient change, as shown in Fig. 3.4 (c).

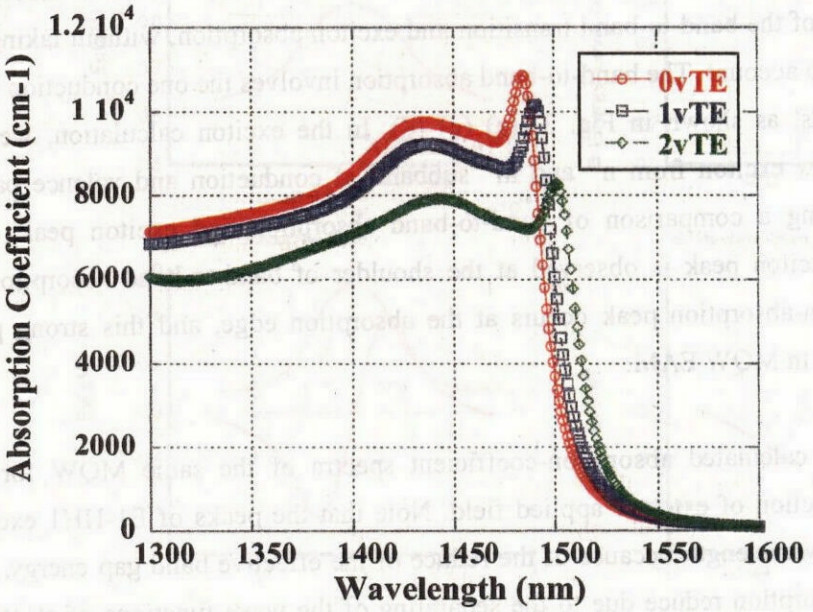

Fig.3.3 Calculated absorption-coefficient spectra of a 7-nm-wide lattice-matched InGaAlAs /InGaAlAs multiple quantum well for TE polarization, as the function of external applied field.

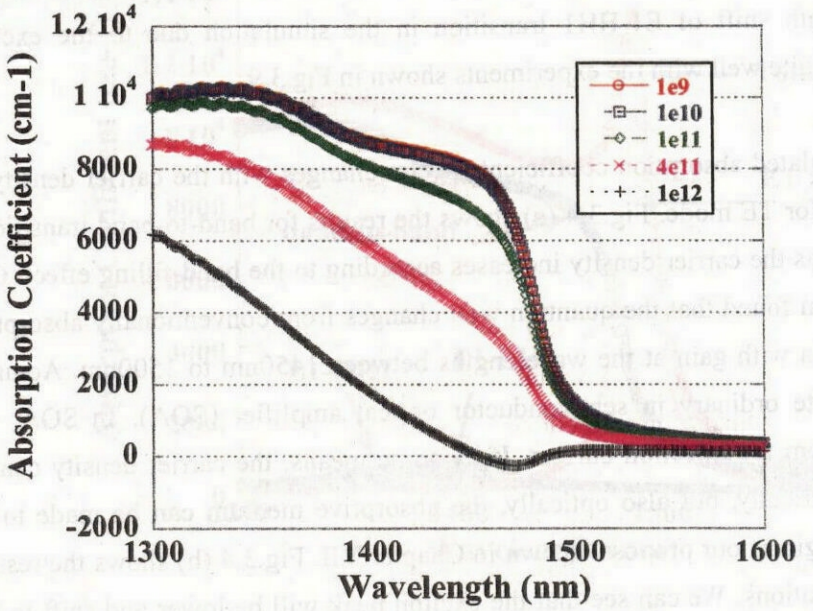

(a)

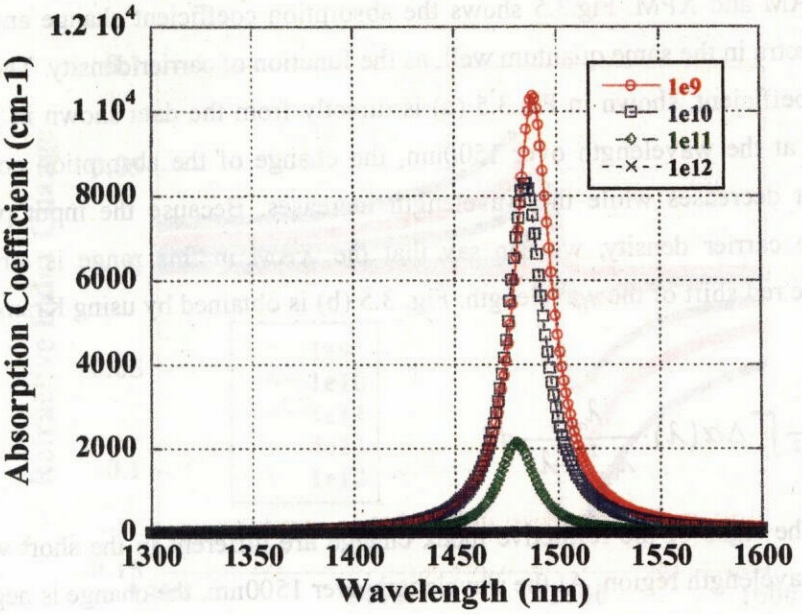

(b)

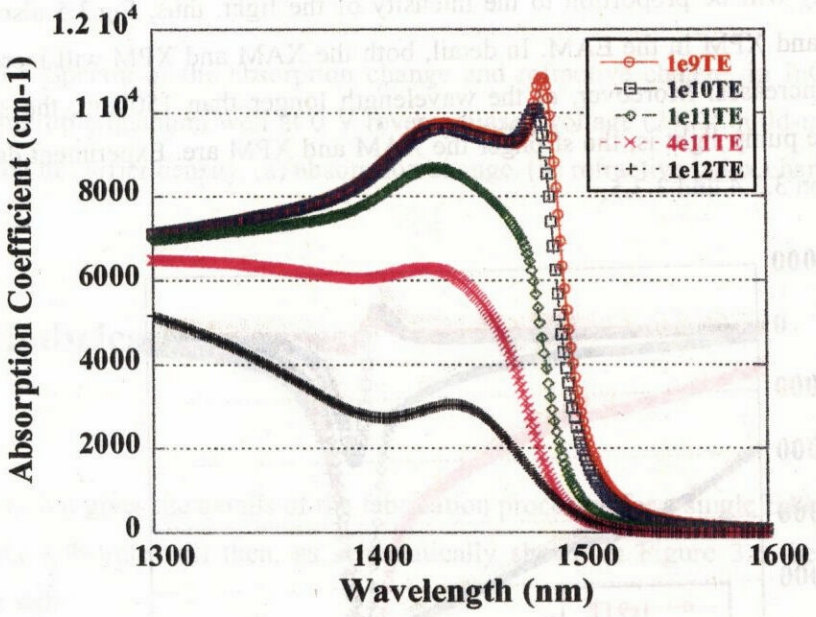

(c)

Fig.3.4 TE-mode absorption coefficient change spectra in InGaAlAs/InGaAlAs 1.45 um multiple quantum well at 0 V reverse biased voltage (21kV build-in electric field), as the function of carrier density. (a). band-to-band absorption. (b). exciton absorption. (c) total absorption

What we care mostly about is the nonlinearity of quantum well. Based on Fig.3.4 we can obtain the results of XAM and XPM. Fig.3.5 shows the absorption coefficient change and refractive index change spectra in the same quantum well, as the function of carrier density. The change of the absorption coefficient, shown in Fig.3.5 (a) is directly from the data shown in Fig.3.4 (c). We can see that at the wavelength over 1500nm, the change of the absorption coefficient is significant and it decreases while the wavelength increases. Because the input power is in proportion to the carrier density, we can say that the XAM in this range is strong and it decreases with the red shift of the wavelength. Fig. 3.5 (b) is obtained by using Kramers-Kronig relation:

$$\Delta n(\lambda_{op}) = \frac{1}{2\pi^2}\int_0^{\infty} \Delta\alpha(\lambda)\cdot\frac{\lambda_{op}^{\ 2}}{\lambda_{op}^{\ 2}-\lambda^2}d\lambda \qquad (3.1)$$

We can see that the signs of the refractive index change are different in the short wavelength region and long wavelength region. At the wavelength over 1500nm, the change is negative, and the change of the refractive index decreases with the increase of wavelength. It is quite similar with that of absorption coefficient. If only the injected light generates the carrier density, then the carrier density will be proportion to the intensity of the light, thus, Fig.3.5 also gives the effects of XAM and XPM in the EAM. In detail, both the XAM and XPM will increase when the pump light increases. Moreover, at the wavelength longer than 1500nm, the shorter the wavelength of the pump light is, the stronger the XAM and XPM are. Experiment data will be given in subsection 3.3.4 and 3.3.5.

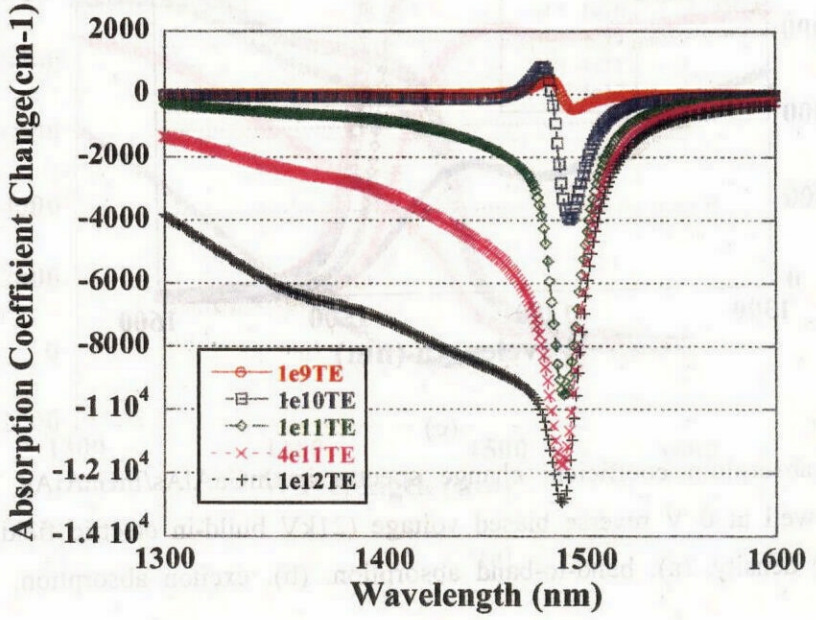

(a)

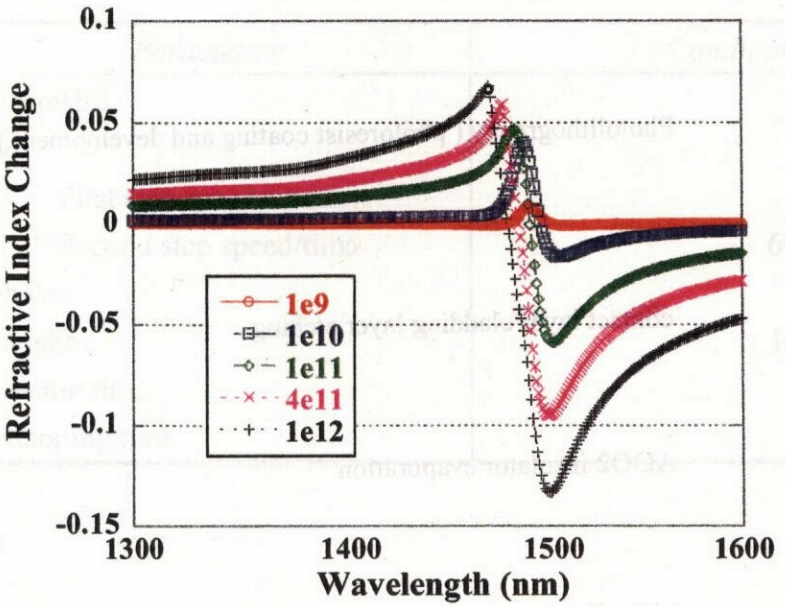

(b)

Fig.3.5 Spectra of the absorption change and refractive change, in InGaAlAs/InGaAlAs 1.45 um multiple quantum well at 0 V reverse biased voltage (21kV build-in electric field), as the function of carrier density. (a) absorption change. (b) refractive index change.

3.2 Fabrication process

This subsection gives the details of the fabrication processes for a single EAM. After the crystal growth, the substrate will then, as schematically shown in Figure 3.6, be processed by the following steps.